Observation of cyclotron resonance and measurement of the hole mass in optimally-doped $La_{2-x}Sr_xCuO_4$

K. W. Post¹, A. Legros², D. G. Rickel¹, J. Singleton¹, R. D. McDonald¹, Xi He^{3,4}, I. Božović^{3,4}, X. Xu^{3,5}, X. Shi⁵, N. P. Armitage^{2,6*}, S. A. Crooker^{1*}

¹National High Magnetic Field Laboratory, Los Alamos National Laboratory, Los Alamos, NM 87545

²Department of Physics and Astronomy, The Johns Hopkins University, Baltimore, MD 21218

³Brookhaven National Laboratory, Upton, NY 11973, USA

⁴Department of Chemistry, Yale University, New Haven, CT 06520, USA

⁵Department of Physics, University of Texas at Dallas, Richardson, TX 75080, USA and

⁶Canadian Institute for Advanced Research, Toronto, Ontario M5G 1Z8, Canada

(Dated: April 14, 2021)

Using time-domain terahertz spectroscopy in pulsed magnetic fields up to 31 T, we measure the terahertz optical conductivity in an optimally-doped thin film of the high temperature superconducting cuprate $\rm La_{1.84}Sr_{0.16}CuO_4$. We observe systematic changes in the circularly-polarized complex optical conductivity that are consistent with cyclotron absorption of p-type charge carriers characterized by a cyclotron mass of $4.9\pm0.8~m_e$, and a scattering rate that increases with magnetic field. These results open the door to studies aimed at characterizing the degree to which electron-electron interactions influence carrier masses in cuprate superconductors.

The renormalization of effective electronic masses in materials is a well-established consequence of electronelectron and electron-lattice interactions. However, precisely how this renormalization manifests depends on the particular measurement. Angle-resolved photoemission, quantum oscillation studies in high magnetic fields (such as Shubnikov-de Haas or de Haas-van Alphen measurements), and heat capacity all measure masses that reflect the underlying renormalized quasiparticle dispersion 1. In contrast, susceptibility or compressibility measurements are sensitive to electronic correlations, but not electron-phonon renormalizations [1]. In this regard, cyclotron resonance (CR) experiments merit special consideration. Famously, Kohn showed that in Galilean-invariant systems, CR reveals a cyclotron mass $m_c = eB/\omega_c$ (where B is the magnetic field and ω_c is the cyclotron frequency) that is not affected by electron-electron interactions 2. Approximate Galileaninvariance is realized in very low charge density systems (e.g., lightly-doped semiconductors) where the Fermi wavelength greatly exceeds the lattice constant. Here the band mass plays the role of the free electron mass. However, these considerations do not apply in higher density systems (e.g., most metals) where, for example, umklapp scattering can be significant 3. Moreover, finite disorder or even small deviations from parabolicity can cause electron-electron interactions to manifest in the cyclotron mass 4. The key point is that electron-electron correlations can influence effective masses measured by CR very differently in comparison to other experimental methods.

In the widely studied high-temperature superconducting cuprate (HTSC) materials, numerous transport, spectroscopic, and thermodynamic-based studies of effective carrier masses have been reported 5-16. Generally, inferred masses are heavy (of order $1-10\ m_e$, where m_e is the bare electron mass), and tend to increase near optimal doping, likely due to renormalization by underlying electron-electron interactions. As such, CR studies can

complement existing methods and help to disentangle the important role of electronic correlations in HTSCs. In the non-interacting limit the cyclotron mass m_c is simply expressed 17 as $m_c = \frac{\hbar^2}{2\pi} \frac{\partial A}{\partial E}$, where A is the cross-sectional area of the Fermi surface in the plane normal to B. It is also noteworthy that CR places much less stringent requirements on sample quality as compared to most other experimental approaches. Small cyclotron shifts of the frequency-dependent conductivity can be resolved (particularly with the THz experiments described here) even when $\omega_c \tau_t$ is significantly less than unity (τ_t is the transport scattering time). This is in contrast to quantum oscillation studies that – due to the exponential sensitivity of quantum oscillations to scattering - generally require $\omega_c \tau_q$ approaching unity (where τ_q is the quantum or phase scattering time [10]). Moreover, the apparent τ_q deduced from quantum oscillations is sensitive to both all scattering mechanisms and inhomogeneities in carrier density; as a result, the observed τ_q is typically smaller than τ_t 18–20.

However, direct detection of CR in the cuprates has proven challenging. This is because carrier masses are expected to be heavy enough that ω_c is expected to be small ($\lesssim 30~\mathrm{GHz/T}$). Additionally, scattering times even in high-quality HTSC samples are short, typically $\lesssim 1~\mathrm{ps}$ [21-25], so that the low-frequency Drude conductivity peak has a broad linewidth $\gtrsim 1~\mathrm{THz}$. Based on these two considerations it is clear that high magnetic fields (many tens of teslas) are needed to make ω_c sufficiently large so that a cyclotron shift of the broad Drude peak can be experimentally resolved.

To this end, we have combined pulsed magnetic fields with THz time-domain spectroscopy (THz-TDS) to reveal CR of holes in the normal state of a high-quality thin film of optimally-doped La_{1.84}Sr_{0.16}CuO₄. The field dependence of the circularly-polarized complex optical conductivity is consistent with CR and a hole mass $m_{\rm c}=4.9\pm0.8~m_{\rm e}$. Significantly, La_{2-x}Sr_xCuO₄ can

be tuned across the entire phase diagram [16], [26], [27], but quantum oscillations have never been detected in any $La_{2-x}Sr_xCuO_4$ sample, even in fields up to 80 Tesla and in temperatures down to 4 K [28]. These results, therefore, represent the first detection of cyclotron resonance in the normal state of a cuprate superconductor and the first measurement of a cyclotron mass in the $La_{2-x}Sr_xCuO_4$ family of cuprate superconductors. In comparison, quantum oscillation studies of hole-doped cuprates have generally been limited to low temperatures, while still demanding extremely high magnetic fields and exceptionaly clean samples of YBa₂Cu₃O_{7-δ} and $YBa_2Cu_4O_8$ (YBCO) [5, 8], $Tl_2Ba_2CuO_{6+\delta}$, and $HgBa_2CuO_{4+\delta}$ [7] (each of which is limited in its respective doping range). Prior reports of broadband magnetooptics in HTSC materials were performed at low temperatures and low B, and no clear spectroscopic signatures of CR were obtained [29, 30]. Our terahertz measurements demonstrate the capability to measure CR in optimally doped $La_{2-x}Sr_xCuO_4$ at temperatures near T_c , overcoming the experimental constraints that have limited quantum oscillation measurements and opening the possibility of characterizing m_c across the entire phase diagram of a single superconducting compound.

We studied a 53 nm thick La_{1.84}Sr_{0.16}CuO₄ film (hereafter termed LSCO), deposited by atomic layer-bylayer molecular beam epitaxy on a 1 mm thick (001)oriented LaSrAlO₄ substrate. The sample was close to optimal doping, and mutual inductance measurements demonstrated a superconducting transition temperature of 41 K. At this doping level, Hall measurements show a hole-like response [26, 31]. Figure 1a shows the experiment, in which a small pulsed magnet is incorporated into the free-space beam path of a THz-TDS spectrometer. The field is applied along the film's (001) direction, which is the same as the light propagation direction (i.e., the Faraday geometry). The magnet has a 15 mm bore and consists of 144 windings of high-strength CuAg wire, and is powered by a purpose-built 20 kJ capacitor bank. The field profile of a 31 T pulse is shown in Fig. 1b. To rapidly detect the THz waveform at peak field, we used a THz-TDS system based on electronically-controlled optical sampling (ECOPS) 32, 33, wherein the timing delay between the two ultrafast optical pulse trains that drive the THz emitter and receiver can be electronically modulated very quickly (see Fig. 1c). When synchronized to the magnetic field, the THz waveform can be recorded at multiple field values during a single magnet pulse. Following standard procedure, the measured THz electric field was Fourier-transformed to yield the frequencydependent complex optical transmission $T(\omega, B)$, which is normalized to the zero-field transmission $T(\omega, 0)$. Signal to noise was further improved by averaging ≈ 20 magnet pulses for each displayed spectrum.

Crucial to this experiment, we measure the complex conductivity of the LSCO film in the right- and left-circularly polarized bases, which are the natural eigenstates of cyclotron motion $[i.e., \sigma_r(\omega)]$ and $\sigma_l(\omega)$, the

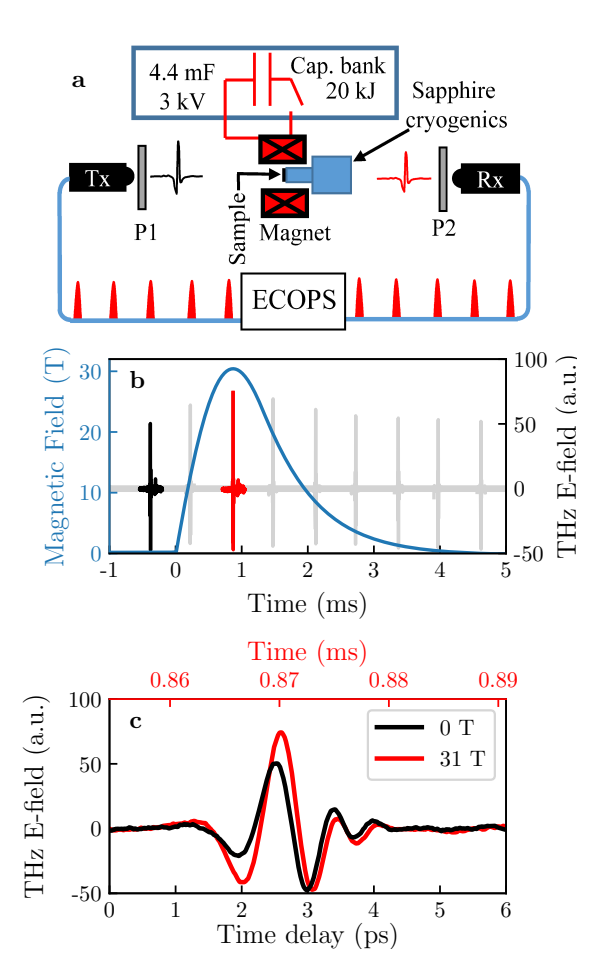


FIG. 1. a) Experimental schematic. A small pulsed magnet is incorporated into the beam path of an ECOPS-based time-domain terahertz spectrometer. Broadband THz optical pulses generated by the transmitter (T_x) are linearly polarized (by P1) and focused through the sample in the magnet bore, and then directed through a second polarizer (P2) and detected by gated receiver (R_x). Parabolic collimating and focusing mirrors are not shown. b) Field profile of a 31 T magnet pulse (blue, left axis) is plotted along with the simultaneously-measured THz electric field (right axis). c) THz electric field measured at zero field (black) and at 31 T (red). The upper x-axis shows actual laboratory time. The ECOPS system sweeps the effective time delay through 5 ps in $\approx 30~\mu s$.

cyclotron-active and -inactive modes, respectively]. As shown below this allows us to unambiguously resolve small cyclotron frequency shifts of the optical conductivity even in the regime where $\omega_c \tau_t < 1$. This is not possible using conventional infrared spectroscopy that does not measure complex transmission coefficients. Here we obtain $\sigma_r(\omega)$ and $\sigma_l(\omega)$ by measuring both diagonal and off-diagonal complex transmission components $T_{xx}(\omega)$ and $T_{xy}(\omega)$. Access to T_{xy} is achieved by incorporating two linear polarizers into the THz beam path (P1 and P2). When P2 is rotated $\pm 45^{\circ}$ with respect to P1, then $T_{\pm 45^{\circ}} = (T_{xx} \pm T_{xy})/\sqrt{2}$, from which we can extract T_{xy} and T_{xx} , and reconstruct the complex con-

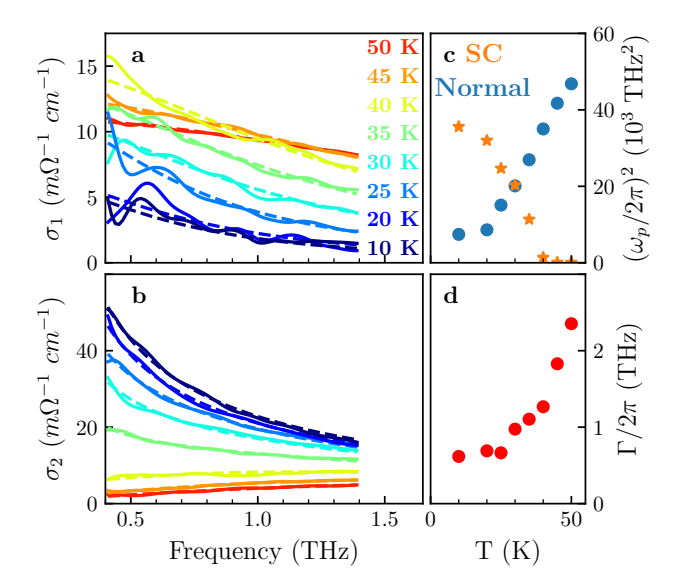


FIG. 2. a,b) The real and imaginary optical conductivity (σ_1 and σ_2 respectively) of the LSCO x=0.16 film at zero magnetic field, at different temperatures. Dashed lines show fits to the spectra following Eq. 1. c) Extracted spectral weight of the normal and superconducting carriers. d) Extracted scattering rate Γ of the normal carriers.

ductivity $\sigma_{r,l}(\omega)$ from the right- and left-circular complex transmission $T_{r,l} = T_{xx} \pm i T_{xy}$ as described in Ref. [34]. Further details on reference measurements characterizing the substrate and depolarization effects of the optics are included in the Supplemental Material [35]. Note that the ability to reconstruct the complex $T_{r,l}$ in a broadband fashion is a capability unique to THz-TDS and is, as shown below, essential to extracting ω_c in this material.

Figures 2a and 2b show the real and imaginary parts of the complex conductivity (σ_1 and σ_2 , respectively) of the LSCO sample at different temperatures at zero field. Upon cooling from 50 K to 40 K, there is a sharpening of the Drude conductivity peak in $\sigma_1(\omega)$, typical of a metal with a decreasing scattering rate Γ . With further cooling to 5 K, the Drude peak loses spectral weight while $\sigma_2(\omega)$ exhibits a $1/\omega$ dependence that increases in magnitude. These are well-established hallmarks of superconductivity, and can be described by a two-fluid model applied to the conductivity, as successfully implemented in many previous studies of the cuprates 21 36 37:

$$\sigma(\omega) = i\epsilon_0 \left(\frac{\omega_{\rm p,n}^2}{\omega + i\Gamma} + \frac{\omega_{\rm p,s}^2}{\omega} - \omega(\epsilon_{\infty} - 1) \right).$$
 (1)

Here, $\omega_{\rm p,n}^2$ and $\omega_{\rm p,s}^2$ are the spectral weights (\propto plasma frequency squared) associated with the normal and superconducting carrier densities $n_{\rm n}$ and $n_{\rm s}$, Γ is the scattering rate of the normal carriers and ϵ_{∞} is the background dielectric constant that arises from excitations at frequencies much higher than our measurement range. Note the use of a frequency independent scattering rate

is justified at our low frequencies, as any frequency dependence over our spectral range is much smaller than the scattering rate's overall scale. Fits are indicated by the dashed lines, and the extracted spectral weights and Γ are shown in Figs. 2c and 2d. The simultaneous reduction of $\omega_{\rm p,n}^2$ and increase of $\omega_{\rm p,s}^2$ with decreasing temperature reveals the condensation of normal carriers into superconducting Cooper pairs. The point at which $\omega_{\rm p,s}^2$ vanishes corresponds to $T_{\rm c}$ (\approx 40 K). The values of Γ (even up to $T_{\rm c}$) are consistent with those obtained in similar high-quality thin films 21, while the values of ω_p^2 are in close agreement with previous infrared studies of La_{2-x}Sr_xCuO₄ 38, 39.

A cyclotron shift of the optical conductivity in a magnetic field is most easily observed by plotting $\sigma_r(\omega)$ and $\sigma_l(\omega)$, the cyclotron-active and -inactive modes, on the same axis using positive and negative values of frequency, respectively. In the simplest model of CR, the real (σ_1) and imaginary (σ_2) conductivities then take the form illustrated in Figs. \mathfrak{J}_a ,b. At B=0 the Drude conductivity peak appears as a single Lorentzian oscillator centered at zero frequency with width Γ . Applied fields B simply shift the Drude peak from zero to ω_c , as depicted \mathfrak{J}_a \mathfrak{J}_c . However, if Γ also increases with B, then σ_1 and σ_2 are additionally broadened and reduced in amplitude as shown in Figs. \mathfrak{J}_c ,d.

Figures 3e and 3f show the experimentally-measured complex conductivity, at 45 K (above T_c), at selected magnetic fields up to 31 T. As field is increased, the data exhibit a small but clear shift of the peak position in the real part of the conductivity, accompanied by a reduction of the peak amplitude, similar to the model depicted in Figs. 3c,d. To quantify the observed behavior, we fit these spectra using a modified two-fluid model that includes a cyclotron shift ω_c :

$$\sigma_{r,l}(\omega) = i\epsilon_0 \left(\frac{\omega_{\rm p,n}^2}{\omega - \omega_{\rm c} + i\Gamma} + \frac{\omega_{\rm p,s}^2}{\omega} - \omega(\epsilon_{\infty} - 1) \right). \quad (2)$$

Note that the sign of ω_c depends on the sign of the charge, and that $\sigma_r(\omega)$ and $\sigma_l(\omega)$ are defined for positive and negative frequencies, as described above. For completeness we retain the small $\omega_{p,s}^2$ term to account for inertial effects of the fluctuating superconductivity that can exist in these samples at small B and slightly above T_c 27, but note that the majority of our data comes from temperatures and magnetic fields that are well above the superconducting transition, where the superconducting contribution is negligible. The sensitivity of the fits to the corrective term in ϵ_{∞} is completely negligible and this term is therefore kept constant during the fitting procedure. Best fits are shown by the dashed lines (fits to all data sets are shown in Fig. 4 and the measured values of ω_c are plotted in Fig. 3g. A linear fit of ω_c to B indicates a relatively heavy carrier mass $m_c \approx 4.7 m_e$ at 45 K. To confirm this result, Fig. 3g also shows results of additional measurements performed at nearby temperatures and plotted in Fig. 4, each yielding similar mass values, which together imply $m_{\rm c}=4.9\pm0.8$

 $m_{\rm e}$. The linear-in-B dependence of ω_c observed at all temperatures is consistent with cyclotron resonance and supports the absence of field-induced Fermi surface reconstructions at x=0.16 up to 31 T (which would result in a deviation from this linear behavior). Note that it was essential here to measure the complex conductivity in the circular basis to resolve the small frequency shift of the conductivity peak. Because of the peak's comparatively large width, measurements sensitive only to σ_{xx} would have shown primarily a drop in the peak amplitude and a broadening, but not a shift.

Finally, the extracted spectral weights of the normal and superconducting carriers are shown in Fig. 5a and the scattering rates in Fig. 5b. With increasing B, $\omega_{\rm p,n}^2$ increases and saturates near the same value for all measured temperatures, while $\omega_{\rm p,s}^2$ is suppressed to zero, as expected for field-induced suppression of superconductivity. Concomitantly, the extracted scattering rate Γ (Fig. 5b) is found to increase with B, by an amount that is temperature-dependent. The field dependence of Γ can also be directly seen in the conductivity spectra of Fig. 3e, via the amplitude reduction and broadening of $\sigma_1(\omega)$ as B increases. To further affirm the reliability of our model fits, we show the DC resistivity derived from our model fit alongside transport data in Fig. 5c, which reveal a remarkable quantitative agreement (discussed further below).

These results represent the first direct measurement of CR in the $La_{2-x}Sr_xCuO_4$ system. Comparing this hole effective mass $(4.9 m_e)$ to values obtained from quantum oscillation studies in other HTSC materials, it is larger than the mass inferred in optimally-doped YBCO $(3.6 m_e)$ 10, and is closer to values obtained in highly overdoped $\text{Tl}_2\text{Ba}_2\text{CuO}_{6+\delta}$ (4.1 m_e) 6. We note that hole masses previously estimated in LSCO from studies that combined zero-field optics and Hall effect data $(\approx 4 m_e)$ 39 are comparable to our measured m_c . It is also in broad agreement with the reported Sommerfeld coefficient of electronic heat capacity 14, 44, 45. Furthermore, a comparison of the observed cyclotron effective mass with photoemission and electrical transport experiments 41, 42 can be made via a tight-binding parameterization of the band structure [43]. At a Fermi energy corresponding to 16% hole doping, such comparisons predict a cyclotron mass of 5.3 m_e (see also Supplemental Material [35]). It is important to note that this treatment potentially misses renormalization occurring at very low energies close to $E_{\rm F}$, and near renormalization "hot-spots" at other regions in the Brillouin zone. Given that these different experimental determinations of effective mass are in principle subject to differing degrees of mass renormalization, the extent to which the masses measured through CR agree with those extracted from other techniques - particularly in various regions of the phase diagram – should be an important topic for future

In addition to the carrier masses, other important parameters extracted from these THz studies (such as the

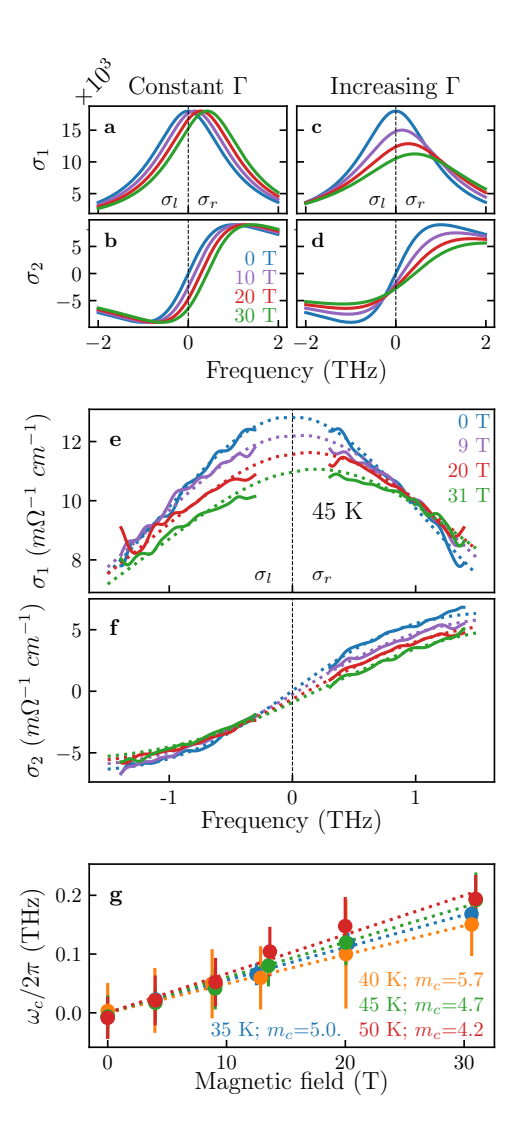


FIG. 3. a,b) Example of circularly-polarized complex conductivity for a model system exhibiting simple CR (using $m_c=2~m_e,~\Gamma=1~\text{THz}$, and a fixed spectral weight). Negative and positive frequencies correspond to $\sigma_l(\omega)$ and $\sigma_r(\omega)$, respectively. Shown in this way, the Drude peak appears as a Lorentzian oscillator centered about $\omega_c=eB/m_c.$ c,d) Same, except now Γ increases linearly from 1.0 to 1.6 THz as $B\to 30~\text{T}$. The Lorentzian conductivity peak now also broadens and diminishes in amplitude with increasing B. e,f) Experimentally measured optical conductivity from LSCO up to 31 T, at 45 K. A clear cyclotron shift is observed, along with an amplitude reduction and broadening consistent with increasing Γ. Dashed lines show fits using a cyclotron-active two-fluid model. g) The extracted values of ω_c . Linear fits to $\omega_c(B)$ reveal the cyclotron mass m_c .

scattering rate Γ) can be compared to values obtained by complementary methods, such as electrical transport. Figure be shows a comparison between Γ extracted from our THz studies, and the resistivity $\rho(B)$ (dashed lines) reported in a similar LSCO film at similar temperatures [28]. Both $\Gamma(B)$ and $\rho(B)$ follow the same general trends, implying that these quantities are closely related. With

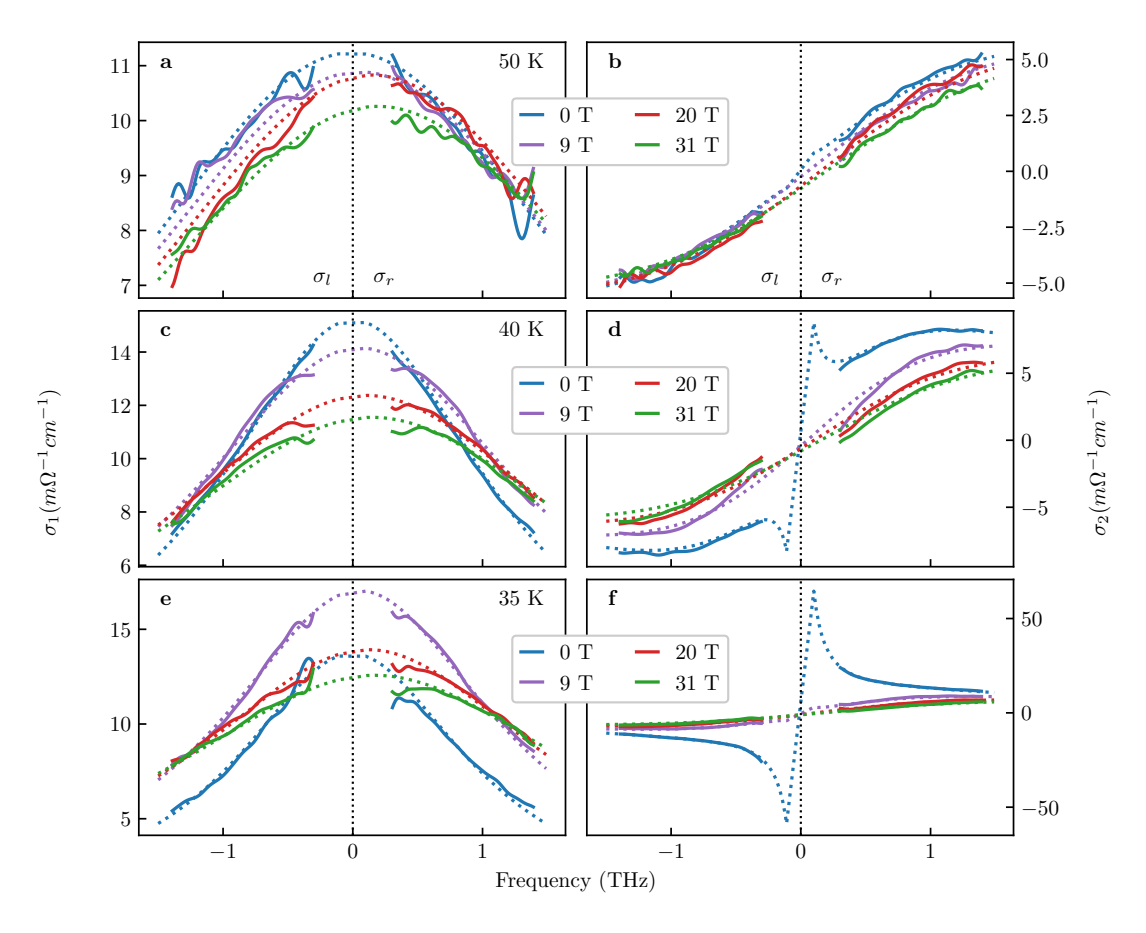


FIG. 4. Field-dependent optical conductivity at different temperatures near T_c , with the real and imaginary components of the complex conductivity shown in the left and right panels, respectively. Data are plotted for a series of increasing magnetic fields, along with model fits (dashed lines). In all these figures, negative and positive frequencies correspond to the optical conductivity measured for left- and right-circularly polarized THz light, respectively. The trends associated with cyclotron resonance observed at 45 K are also observed at 50 K. They persist as well at lower temperatures, while the lineshapes sharpen due to the decreasing scattering rate. Additionally, at 35 K (and to a lesser extent at 40 K) there is an expected divergence of σ_2 at 0 T (panel f) that is rapidly suppressed with increasing magnetic field. Concomitantly, the peak amplitude in σ_1 (panel e) increases with applied field. These features are both consistent with the field-induced suppression of superconducting carriers. Importantly, the features in all spectra are captured very well by the modified two-fluid model.

further analysis, this observation could help distinguish between competing models for the distinctive normalstate magnetoresistance of cuprates [46]. We present in Fig. 5c an additional comparison, between the same dc resistivity determined by magneto-transport measurements and the resistivity obtained from our fits of the conductivity, i.e. $1/\sigma_1(\omega \to 0)$ where $\sigma_1(\omega \to 0)$ is the zero frequency value of the real part of the conductivity anticipated from our model. Although these two different techniques were applied to samples of slightly different doping, the transport resistivity values differ by only 20% compared to the dc resistivity estimated from optics. This close agreement between optical- and transportbased measurements affirms the validity of our model fits and hints at underlying universality within these LSCO thin films. Using the values obtained at maximum field (31 T) of ω_c and $\omega_{p,n}$, we can estimate the dc Hall effect as well, via the expression $R_H = \omega_c/(\epsilon_0 \omega_{p,n}^2 H)$ for the normal state: at a temperature of 35 K, we obtain

 $R_H = 2.2 \pm 0.2 \text{ mm}^3/\text{C}$ (corresponding to a Hall number $n_H = V/eR_H \simeq 0.27$).

To conclude, we have observed the first clear signature of cyclotron resonance in a HTSC, in the normal state of LSCO close to optimal doping. Using time-domain THz spectroscopy coupled to pulsed magnetic fields up to 31 T, we were able to measure a cyclotron shift in the conductivity up to temperatures of 50 K in this relatively disordered hole-doped cuprate. These experimental conditions are less restrictive than quantum oscillation measurements and therefore allow for the study of a much broader range of cuprates. The quantities extracted from our fits of the conductivity such as cyclotron mass and estimated dc resistivity are in broad agreement with other types of experiments, and the linear field-dependence of the cyclotron frequency indicates the absence of fieldinduced Fermi surface reconstructions at this doping up to 31 T. Further analysis and comparison of the cyclotron mass (especially with additional m_c values over a wide

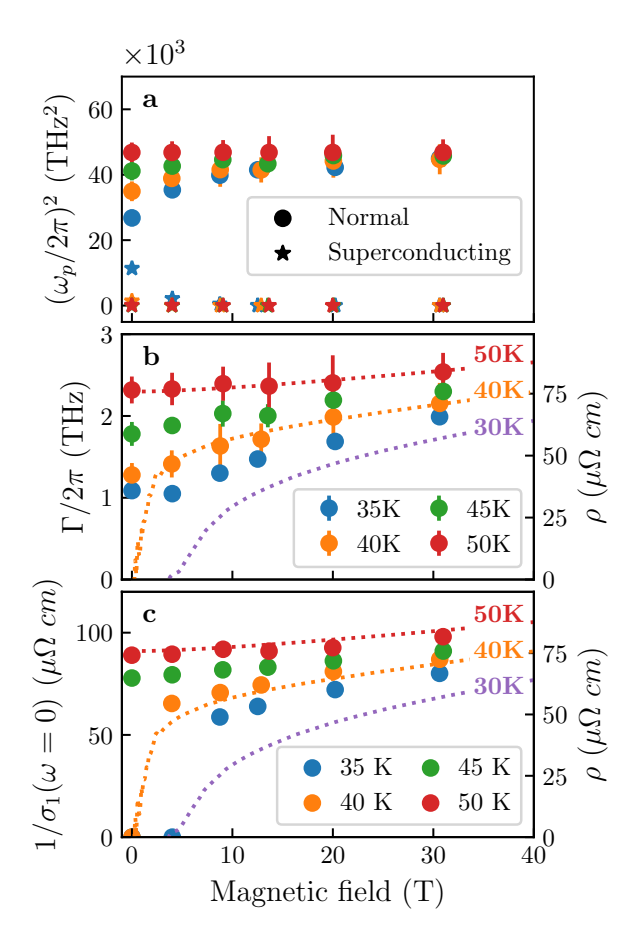


FIG. 5. a) Magnetic field dependence of the spectral weights $\omega_{\mathrm{p,n}}^2$ and $\omega_{\mathrm{p,s}}^2$ at all measured temperatures. $\omega_{\mathrm{p,s}}^2$ decreases as superconductivity is suppressed by B, while $\omega_{\mathrm{p,n}}^2$ increases. b) The scattering rate Γ increases with B at all measured temperatures. Also shown is ρ (dotted lines, right axis), the resistivity measured in a similarly-doped LSCO thin film, at 50, 40, and 30 K (from [28]). c) Comparison between the same resistivity from [28] (dotted lines, right axis) and the DC resistivity extracted from our fits to the optical conductivity (colored circles, left axis) at different temperatures. In this panel we use $1/\sigma_1(\omega=0)=0$ for data points at $T=40\mathrm{K}$ in zero field and $T=35\mathrm{K}$ at 4T to reflect the presence of superconductivity at these temperatures and fields (since we measure a non-zero $\omega_{\mathrm{p,s}}$ for these data points).

doping range) to masses extracted with different types of experiments may help characterize the degree to which electron-electron interactions influence carrier masses in cuprates. We emphasize that LSCO can be advantageously tuned across its entire doping range, in contrast to other hole-doped cuprates in which quantum oscillations have been measured (YBCO, $HgBa_2CuO_{4+\delta}$, and $Tl_2Ba_2CuO_{6+\delta}$), and that samples away from the optimal doping and therefore with a lower T_c would enable access to the normal state at lower temperatures where CR is expected to be more prominent. In this way, the successful measurement of $\omega_{\rm c}$ demonstrated in this work paves the way for future studies aimed at characterizing the full doping dependence of extracted quantities such as m_c . We note that both the van Hove singularity in the band structure 47, 48 at a doping $p \approx 0.19 \approx p*$ (the pseudogap critical point in LSCO [49]), and the reported divergence of the electronic heat capacity in the same doping region 14, 45, suggest a rapidly-varying effective mass in this doping range. Thus, CR measurements are well positioned to shed light on the role of single-particle vs. many-body renormalization effects in the cuprates (moreover, equivalently small scattering rates have already been realized in the overdoped region of LSCO [21]). Combined with direct measurement of Γ at temperatures above and below $T_{\rm c}$ that are enabled by THz-TDS, such results have the potential to bring new insights into "strange metal" phenomena such as Tlinear and B-linear resistivity at low temperatures close to p* [28], and the role of quantum criticality in shaping the superconducting dome. We therefore encourage further theoretical investigations of cyclotron resonance phenomena in correlated systems.

Work at the National High Magnetic Field Laboratory was supported by National Science Foundation (NSF) DMR-1644779, the State of Florida, and the U.S. Department of Energy (DOE). AL and NPA were supported by the Quantum Materials program at the Canadian Institute for Advanced Research and NSF DMR 1905519. Work at Brookhaven National Laboratory was supported by the DOE, Basic Energy Sciences, Materials Sciences and Engineering Division. X. H. is supported by the Gordon and Betty Moore Foundation's EPiQS Initiative through grant GBMF9074. We gratefully acknowledge G. Granroth for providing the CuAg wire used in our pulsed magnet, and S. Chakravarty, J. Chang, S. Chen, M. Horio, S. Kivelson, B. Ramshaw, A. Shekter, Z. X. Shen, and L. Taillefer for helpful conversations.

^[1] D. Pines and P. Nozieres, *The Theory of Quantum Liquids* (W. A. Benjamin, New York, 1966).

^[2] W. Kohn, Phys. Rev. **123**, 1242 (1961).

^[3] K. Kanki and K. Yamada, J. Phys. Soc. Jpn. 66, 1103 (1997).

^[4] A. H. MacDonald and C. Kallin. Phys. Rev. B 40, 5795, (1989).

^[5] N. Doiron-Leyraud, C. Proust, D. LeBoeuf, J. Levallois, J. Bonnemaison, R. Liang, D. A. Bonn, W. N. Hardy,

and L. Taillefer, Nature 447, 565 (2007).

^[6] B. Vignolle, A. Carrington, R. A. Cooper, M. M. J. French, A. P. Mackenzie, C. Jaudet, D. Vignolles, Cyril Proust, and N. E. Hussey, Nature 455, 952 (2008).

^[7] N. Barišić, S. Badoux, M. K. Chan, C. Dorow, W. Tabis, B. Vignolle, G. Yu, J. Béard, X. Zhao, C. Proust, and M. Greven, Nat. Phys. 9, 761 (2013).

^[8] S. E. Sebastian and C. Proust, Ann. Rev. Cond. Matt. Phys. 6, 411 (2015).

- [9] B. J. Ramshaw, B. Vignolle, J. Day, R. Liang, W. N. Hardy, C. Proust, and D. A. Bonn, Nat. Phys. 7, 234 (2011).
- [10] B. J. Ramshaw, S. E. Sebastian, R. D. McDonald, James Day, B. S. Tan, Z. Zhu, J. B. Betts, R. Liang, D. A. Bonn, W. N. Hardy, and N. Harrison, Science 348, 317 (2015).
- [11] T. Helm, M. V. Kartsovnik, M. Bartkowiak, N. Bittner, M. Lambacher, A. Erb, J. Wosnitza, and R. Gross, Phys. Rev. Lett. 103, 157002 (2009).
- [12] J. S. Higgins, M. K. Chan, T. Sarkar, R. D. McDonald, R. L. Greene and N. P. Butch, New J. of Phys. 20, 043019 (2018).
- [13] J. W. Loram, K. A. Mirza, J. M. Wade, J. R. Cooper, W. Y. Liang, Physica C 235-240, 134 (1994).
- [14] B. Michon, C. Girod, S. Badoux, J. Kačmarčík, Q. Ma, M. Dragomir, H. A. Dabkowska, B. D. Gaulin, J.-S. Zhou, S. Pyon, T. Takayama, H. Takagi, S. Verret, N. Doiron-Leyraud, C. Marcenat, L. Taillefer, and T. Klein, Nature 567, 218 (2019).
- [15] C. Girod, A. Legros, A. Forget, D. Colson, C. Marcenat, A. DeMuer, D. LeBoeuf, L. Taillefer, and T. Klein, Phys. Rev. B 102, 014506 (2020)
- [16] A. Ino, C. Kim, M. Nakamura, T. Yoshida, T. Mizokawa, A. Fujimori, Z.-X. Shen, T. Kakeshita, H. Eisaki, and S. Uchida, Phys. Rev. B 65, 094504 (2002).
- [17] N. Ashcroft and D. Mermin, Introduction to Solid State Physics (1976).
- [18] M. V. Kartsovnik, Chem. Rev. 104, 5737 (2004).
- [19] J. Singleton, Band Theory and Electronic Properties of Solids, (Oxford, 2001).
- [20] N. Harrison and J. Singleton, J. Phys.: Condens. Matter 13, L463 (2001).
- [21] F. Mahmood, X. He, I. Božović, and N. P. Armitage, Phys. Rev. Lett. 122, 027003 (2019).
- [22] J. Corson, J. Orenstein, Seongshik Oh, J. O'Donnell, and J. N. Eckstein, Phys. Rev. Lett. 85, 2569 (2000).
- [23] T. Valla, A. V. Fedorov, P. D. Johnson, Q. Li, G. D. Gu, and N. Koshizuka, Phys. Rev. Lett. 85, 828 (2000).
- [24] N. E. Hussey, Eur. Phys. J. B 31, 495 (2003).
- [25] B. J. Ramshaw, N. Harrison, S. E. Sebastian, S. Ghannadzadeh, K. A. Modic, D. A. Bonn, W. N. Hardy, Ruixing Liang, and P. A. Goddard, npj Quantum Materials 2, 8 (2017).
- [26] Y. Ando, Y. Kurita, S. Komiya, S. Ono, and K. Segawa, Phys. Rev. Lett. 92, 197001 (2004).
- [27] L. S. Bilbro, R. Valdés Aguilar, G. Logvenov, O. Pelleg, I. Božović, and N. P. Armitage, Nat. Phys. 7, 298 (2011).
- [28] P. Giraldo-Gallo et al., Science **361**, 479 (2018).
- [29] S. Spielman, B. Parks, J. Orenstein, D. T. Nemeth, F. Ludwig, J. Clarke, P. Merchant, and D. J. Lew, Phys. Rev. Lett. 73, 1537 (1994).
- [30] H. D. Drew, E. Choi, and K. Karrai, Physica B 197, 624

- (1994).
- [31] F. F. Balakirev, J. B. Betts, A. Migliori, I. Tsukada, Y. Ando, and G. S. Boebinger, Phys. Rev. Lett. 102, 017004 (2009).
- [32] R. J. B. Dietz, N. Vieweg, T. Puppe, A. Zach, B. Glo-bisch, T. Göbel, P. Leisching, and M. Schell, Opt. Lett. 39, 6482 (2014).
- [33] G. T. Noe, Q. Zhang, J. Lee, E. Kato, G. L. Woods, H. Nojiri, and J. Kono, Appl. Opt. 53, 5850 (2014).
- [34] B. Cheng, P. Taylor, P. Folkes, C. Rong, and N. P. Armitage, Phys. Rev. Lett. 122, 097401 (2019).
- [35] See Supplemental Material at [URL will be inserted by publisher] for calculations of effective mass from photoemission and transport parameters, and for control THz experiments.
- [36] D.N. Basov and T. Timusk, Rev. Mod. Phys. 77, 2 (2005).
- [37] M. Tinkham. Introduction to Superconductivity (Dover, 2004).
- [38] S. Uchida, T. Ido, H. Takagi, T. Arima, Y. Tokura, and S. Tajima, Phys. Rev. B 43, 7942 (1991)
- [39] W. J. Padilla, Y. S. Lee, M. Dumm, G. Blumberg, S. Ono, K. Segawa, S. Komiya, Y. Ando, and D. N. Basov, Phys. Rev. B 72, 060511 (2005).
- [40] E. D. Palik and J. K. Furdyna, Rep. Prog. Phys. 33, 1193 (1970).
- [41] Y. Fang, G. Grissonnanche, A. Legros, S. Verret, F. Laliberte, C. Collignon, A. Ataei, M. Dion, J. Zhou, D. Graf, M. J. Lawler, P. Goddard, L. Taillefer, and B. J. Ramshaw, arXiv:2004.01725.
- [42] M. Horio et al., Phys. Rev. Lett. 121, 077004 (2018).
- [43] R. S. Markiewicz et al., Phys. Rev. B 72, 054519 (2005).
- [44] N. Momono, M. Ido, T. Nakano, M. Oda, Y. Okajima, K. Yamaya, Physica C 233, 395 (1994).
- [45] C. Girod, D. LeBoeuf, A. Demuer, G. Seyfarth, S. Imajo, K. Kindo, Y. Kohama, M. Lizaire, A. Legros, A. Gourgout, H. Takagi, T. Kurosawa, M. Oda, N. Momono, J. Chang, S. Ono, G.-q. Zheng, C. Marcenat, L. Taillefer, and T. Klein, arXiv:2101.09221.
- [46] J. Singleton, Physical Review Materials 4, 061801 (2020).
- [47] T. Yoshida, M. Hashimoto, S. Ideta, A. Fujimori, K. Tanaka, N. Mannella, Z. Hussain, Z.-X. Shen, M. Kubota, K. Ono, S. Komiya, Y. Ando, H. Eisaki, and S. Uchida, Phys. Rev. Lett. 103, 037004 (2009).
- [48] J. Chang, M. Shi, S. Pailhés, M. Mansson, T. Claesson, O. Tjernberg, A. Bendounan, Y. Sassa, L. Patthey, N. Momono, M. Oda, M. Ido, S. Guerrero, C. Mudry, and J. Mesot Phys. Rev. B 78, 205103 (2008).
- [49] R. A. Cooper, Y. Wang, B. Vignolle, O. J. Lipscombe, S. M. Hayden, Y. Tanabe, T. Adachi, Y. Koike, M. Nohara, H. Takagi, C. Proust, N. E. Hussey, Science 323, 603 (2009).
- [50] E. Pavarini, I. Dasgupta, T. Saha-Dasgupta, O. Jepsen, and O. K. Andersen, Phys. Rev. Lett. 87, 047003 (2001).